catalysts

MDPI

Article

Significance of C_3 Olefin to Paraffin Ratio in Cobalt Fischer–Tropsch Synthesis

Erling Rytter *, Jia Yang, Øyvind Borg † and Anders Holmen

Department of Chemical Engineering, Norwegian University of Science and Technology (NTNU), N-7491 Trondheim, Norway; jia.yang@ntnu.no (J.Y.); ovbo@equinor.com (Ø.B.); anders.holmen@ntnu.no (A.H.)

* Correspondence: rytter@ntnu.no; Tel.:+47-99165709

† Present address: Equinor Research Centre, N-7053 Trondheim, Norway.

Received: 6 July 2020; Accepted: 20 August 2020; Published: 24 August 2020

Abstract: The ratio between propene and propane (C_3 o/p) during Fischer–Tropsch synthesis (FTS) has been analyzed based on both literature reports and experiments for five catalysts. The latter comprise four cobalt catalysts on γ-alumina with variations in pore sizes, and one catalyst on α-alumina. Overall variations include H_2/CO feed ratio, residence time, water addition, transients between test conditions, CO conversion, cobalt particle size, promoter (Re), and support material. It was possible to rationalize all data based on secondary hydrogenation of olefins. In fact, it was deduced that olefins are dominating termination products in FTS, estimated to ca. 90% for C_3, but that some paraffins most likely are also produced directly. Increased residence time and high H2/CO feed ratio favors olefin hydrogenation, while added water presumably displaces hydrogen on cobalt giving enhanced C_3 o/p. High cobalt dispersion favors hydrogenation, as also promoted by Re. Effect of intraparticle diffusion is seen in transient periods; for example, as water is added or depleted. There is frequently positive correlation between C_3 o/p and selectivity to longer chains; the latter expressed as C_{5+} selectivity, as both are sensitive to hydrogen activity. Some modifications, however, are needed due to the accepted volcano plot for C_{5+} selectivity with cobalt crystallite size. Titania as support shows unexpectedly low C_3 o/p; probably due to SMSI (strong-metal-support-interaction).

Keywords: Fischer–Tropsch; catalysis; cobalt; olefins; mechanism; syngas conversion

1. Introduction

Fischer–Tropsch synthesis (FTS) is frequently divided into high-temperature and low-temperature synthesis. The present paper is concerned with low-temperature FT-synthesis (LT-FTS); commonly conducted over a cobalt catalyst in the temperature range 200–250 °C and pressure typically between 10 and 40 bar. Cobalt is supported on a porous material to achieve the desired cobalt crystallite size of 7–20 nm, and a promoter is frequently added to facilitate reduction and dispersion of the active metal. The general reaction in LT-FTS from synthesis gas (syngas) over cobalt catalysts can be described as

$$n\,CO + 2n\,H_2 \rightarrow C_nH_{2n} + n\,H_2O \quad (1)$$

Assuming the primary product to be an olefin, some paraffins may be directly produced as well, but also obtained by secondary hydrogenation of the olefins. The result is that the observed olefin to paraffin ratio (o/p) for a given chain length depends on process conditions as well as on catalyst formulation. In addition to polymerization of CO, ca. 5–10% of the carbon is converted to methane by a separate reaction, while CO_2 produced by water-gas-shift constitutes less than 1%.

From Equation (1), a stoichiometric amount of water is produced for each carbon in the product. In a recent series of papers on cobalt Fischer–Tropsch synthesis [1–3], we have demonstrated that

water is not a silent spectator, but plays a significant role in all parts of FTS; including formation and secondary reaction of olefins. Olefins as products follow from the commonly assumed β-hydrogen elimination reaction from the chain end after insertion of a CH_2* monomer, as depicted in Figure 1a,b. The recently proposed vinylene chain growth mechanism, using CH* as monomer, was proposed by Rytter and Holmen [4]; reference Figure 1c. In this case, the olefin is produced by hydrogenation of the α-atom of the growing chain (Figure 1d). At first sight, it might seem astonishing that an unsaturated product is formed by hydrogenation. The result is, however, that the Anderson–Schultz–Flory (ASF) chain growth probability (α) becomes independent of hydrogen partial pressure; in accordance with the work of Oosterbeek et al. [5]. This complies with the analyses of α-values for a large number of cobalt catalysts on γ-alumina, α-alumina, and titania supports; it was found "unlikely that θ_H would be a major descriptor of higher α_n values" [6].

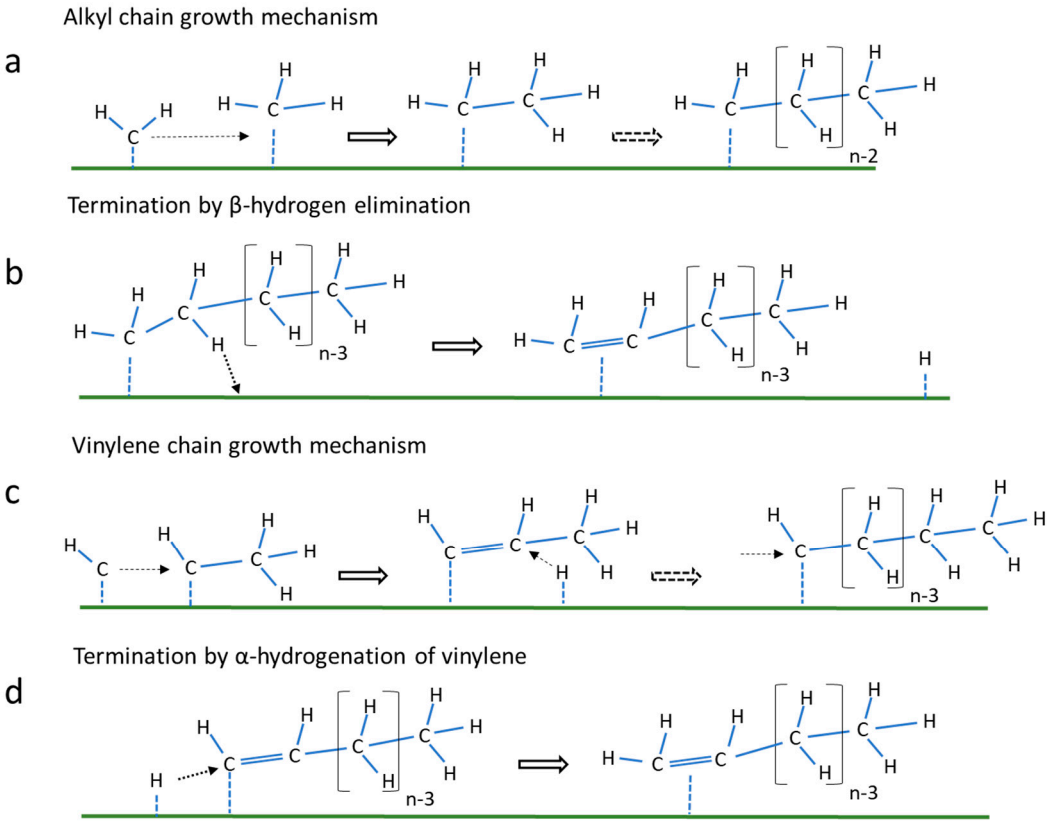

Figure 1. Chain propagation and termination mechanisms for low-temperature Fischer–Tropsch synthesis. (**a**) Alkyl chain growth mechanism; (**b**) Termination by β-hydrogen elimination: (**c**) Vinylene chain growth mechanism; (**d**) Termination by α-hydrogenation of vinylene.

According to the above mechanisms, the primary product of FTS is olefins, and paraffins are mostly produced by secondary hydrogenation. Indeed, this was rationalized in terms of secondary hydrogenation of olefins to paraffins that increases with residence time, chain length, and catalyst particle size [7–9]. In other words, olefins are favored under conditions with short contact times and reduced transport limitations. Further, it follows from the ASF distribution that there is steady decrease in the amount of chains with increasing chain length n; also per carbon atom in the chain. Simultaneously, there is concurrent decrease in the ratio between olefins and paraffins; in other words, in the o/p ratio. There is a notable exception for C_2, both as the total C_2 selectivity is significantly lower than expected, but also because the o/p value is much lower than for consecutive chain lengths. Although the present work does not focus on C_2, it appears that o/p responses with changing process conditions follow higher C_n.

Figure 2 contains a collection of some of the group's reports that contain information on olefin to paraffin ratio. Experiments include; catalysts on a number of different support materials including phases of alumina, γ-alumina with large variation in pore sizes and pore size distributions, titania, silica, and washcoats on a variety of monolithic supports; cobalt with and without rhenium as promoter; different conversion levels; and some with water added to the feed. The variation of C_3 o/p in the figure spans from 0.8 to 3.1, a significant spread compared to the accuracy (2σ) of 0.05–0.1 unit. This indicates that the o/p ratio is a parameter that can be coupled both to catalyst formulation, FT mechanism, and kinetics.

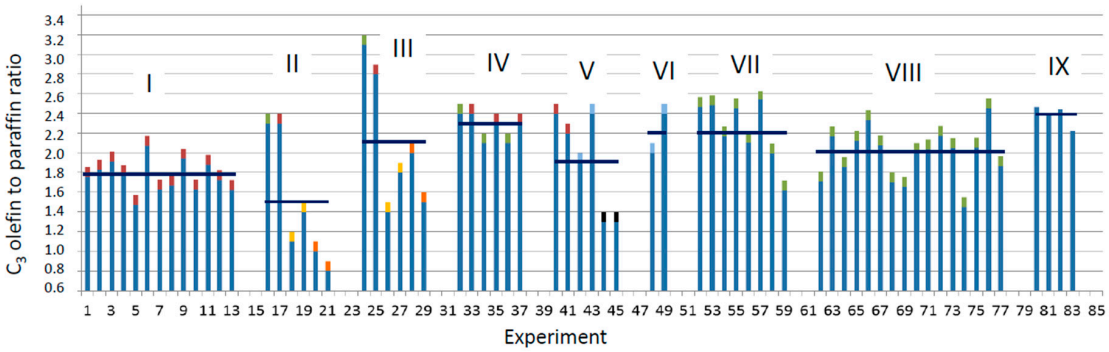

Figure 2. Summary of C_3 olefin to paraffin ratio in cobalt Fischer–Tropsch synthesis from some published works. Color coding of bar tips: Brown: γ-alumina supports; green: without rhenium promoter; black: steel monolith; yellow: silica supports; light brown/orange: titania supports. Experimental series: I: Co/Re on γ-alumina supports with varying pore characteristics [10]; II: Co and Co/Re on γ-alumina, silica and titania supports [11]; III: as II, but initial data at low conversion; IV: Co and Co/Re on γ-alumina with different pore sizes [12]; V: Co/Re on γ-alumina powder and washcoats on cordierite, alumina, and steel monoliths [13]; VI: Co/Re on γ-alumina washcoats on alumina monolith; VII: Co with common crystallite size on different alumina phases [14]; VIII [15]: Co with varying crystallite sizes on different alumina phases; IX: Co/Re with constant crystallite size on different alumina phases (NTNU master thesis). Experimental conditions: Incipient wetness impregnation; 20 bar; 210 °C; H_2/CO: 2.1; CO conversion: 40–45% (except III).

Additional work includes analysis of defects and hcp/fcc phases in Co crystallites. Tsakoumis et al. found that Co nano-particles with minimum number of crystal defects, either due to lattice carbon or stacking faults, have high TOF (turn-over-frequency) and chain-growth probability [16]. These observations were coupled to enhanced surface population of CH_x* and high o/p values (C_3: 3.31 at standard conditions); explained by low relative concentration of hydrogen. In contrast, Lögdberg et al. found negative correlation between STY (site-time-yield) and o/p for a series of γ-alumina supported catalysts, but these were characterized by increasing Co crystallite size [6]. Enger et al. investigated 23 cobalt catalysts on alumina and spinel supports and found that C_3 o/p increases with water vapor pressure [17]. Variations in o/p among the catalysts were discussed in terms of re-adsorption of olefins and surface coverages. Borg et al. found close positive correlation between C_{5+} selectivity and C_3 o/p ratio for 21 catalysts on γ-alumina characterized by different cobalt loading and tuned metal crystallite sizes. They indicated that variations in hydrogenation of olefins activity were the root cause [18].

In their study of Ru, Co, and Fe catalysts at typical FTS conditions, Iglesia et al. [19], and Komaya and Bell [20], concluded that re-adsorption of an olefin followed by chain initiation is the most important secondary reaction instead of hydrogenation (or hydrogenolysis) reactions. As feed space velocity is decreased, the residence time of reactants increases, and CO conversion and water production is enhanced. It is well known that C_{5+} selectivity increases and CH_4 selectivity decreases with higher CO conversion under isothermal conditions. Simultaneously, the olefin to paraffin ratio decreases. The authors claim that the increase in chain growth, and decrease in o/p ratio, is due to the enhanced secondary reaction (re-adsorption and re-initiation) of α-olefins at prolonged bed residence times [21,22].

They also offered a mechanism whereby olefins compete with methyl on the cobalt surface, thereby suppressing methane formation. However, in our opinion it is not obvious that high C_{5+} and low methane selectivities (high CO conversion) occur at conditions where there is low concentration of olefins in the product; rather the contrary. Low selectivity to olefins means low surface concentration of olefins. In contrast to the latter interpretation, Bell and co-workers studied a $Co/Mn/SiO_2$ catalyst and ascribed lower C_2-C_4 o/p ratio with higher CO conversion at low GHSV (gas hourly space velocity) to increased residence time available for hydrogenation of the olefins [23].

Davis and coworkers investigated FTS with unsupported cobalt catalyst in slurry (CSTR) environments and water added. They concluded that water inhibits secondary hydrogenation of ethene with consequently higher C_2 o/p ratios [24]. It can be inferred from one of their figures that secondary hydrogenation is reduced for short residence times. As a model reaction for secondary hydrogenation, Aaserud et al. studied hydrogenation of propene at 120 °C and 1.8 bar for a multitude of supported and unsupported FT catalysts [25,26]. They established that hydrogenation of olefins is suppressed when water is added to the feed, indicating that water competes for hydrogen sites on cobalt. Further, they correlated reduced hydrogenation activity for cobalt on low surface area supports (α-alumina; titania) with increase in C_{5+} selectivity in FTS; and suggested that this was due to re-adsorption of olefins. Todic et al. made a comprehensive study of selectivity effects for a Co/Re/alumina catalyst with changing process conditions and analyzed each component up to C_{15} [27]. There is a small decline in o/p ratio for individual C_3-C_6 chains as the reaction temperature is adjusted from 205 to 230 °C, and as the pressure is increased from 1.5 to 2.5 MPa. Several parameters change during these operations; including CO conversion, water partial pressure, and hydrogen coverage, but it appears that direct influence on the rate of secondary hydrogenation dominates. More distinct are the effects of H_2/CO feed ratio (1.4 and 2.1) and GHSV, in other words, residence time and conversion (24.3 to 54.6%). High hydrogen syngas concentration favors hydrogenation of olefins as do long residence times.

There appears to be ample evidence and agreement in the literature that the olefin/paraffin ratio decreases due to enhanced hydrogenation with:

- Long residence times,
- Low water vapor levels.

This means that for experiments where the CO-conversion is increased by reducing GHSV, there are two opposing effects: o/p decreases due to high residence time; and o/p increases due to higher indigenous water vapor pressure. Of these, the residence time effect is dominating. The co-current increase in C_{5+} selectivity does not necessarily follow, and the often-cited incorporation of olefins into the chain is not needed for explaining changes in the o/p ratio. Yang et al. discussed possible incorporation of olefins into growing chains by considering two types of olefins: desorbed olefins and olefins just produced by chain termination [28]. The former type was discarded based on ^{14}C labeled C_2-C_{19} olefins added to the feed [29–32]; only a small fraction of labeled carbon was detected in the FT-product. The second type, olefins prior to exiting the cobalt surface, the catalyst particle, or both, was examined by deuterium tracer studies. Minimal incorporation into growing chains was also detected in this case [33]. Therefore, chain initiation or incorporation of olefins into the growing FT polymer chain have been disregarded in the present analysis.

Present work is intended as a perspective on olefin to paraffin ratio in FT-catalysis. It can be regarded as a progress account on the subject including consistent interpretation of reported and new data. The paper has been organized into subsections for o/p ratio response to process conditions or catalyst formulation using original data or reanalyzing literature data.

2. Results and Discussion

This section includes reinterpretation or replotting of literature data as well as new experimental data.

2.1. Propene/Propane Response to H_2/CO Feed Ratio

Hydrogenation of olefins will evidently increase with higher H_2/CO feed ratios. This effect is shown in Figure 3 for six ratios; four below the consumption ratio, one close to the consumption ratio of ca. 2.15, and one above. The experiments were conducted by starting with a certain gas flow, and then decreasing the flow rate each day to increase CO conversion. There are three expected responses with time-on-stream (TOS): increased residence time allows more olefins to be hydrogenated; in contrast, high conversion produces more water that can replace hydrogen on the cobalt surface; hydrogen partial pressure can be accumulated or depleted with conversion depending on the initial H_2/CO ratio. The data for H_2/CO = 2.21, in other words, near constant ratio through the fixed-bed reactor, shows steady o/p decline with residence time. Therefore, it is evident that residence time beats any suppression of hydrogenation from produced water. The effect on o/p ratio is enhanced for H_2/CO = 2.55 because hydrogen becomes more abundant with conversion. More significant is the decline in hydrogenation as the H_2/CO ratio is reduced gradually from 1.74 to 1.03. Note that there is no longer a linear response to GHSV (residence time; CO conversion); there is an upward trend for higher CO conversions, and more so for the lowest feed ratio. The observed curvature is due to depletion of hydrogen with conversion that counteracts residence time increase.

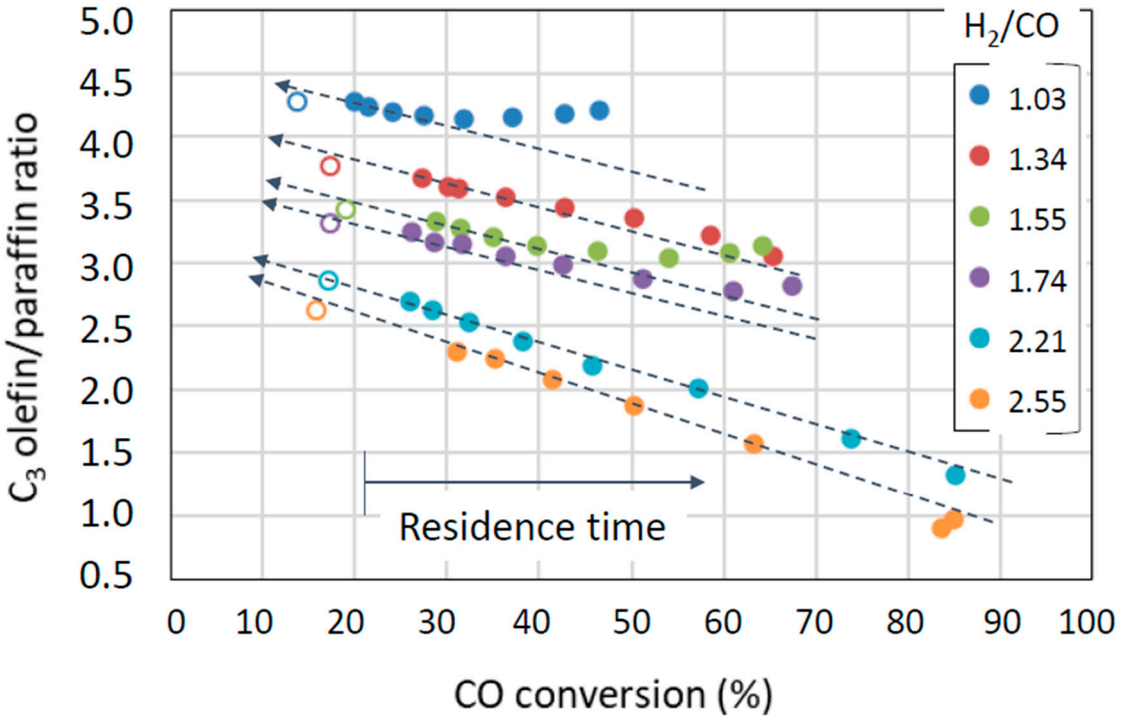

Figure 3. C_3 olefin/paraffin ratios for variations in H_2/CO feed ratio at gradually decreasing GHSV (gas hourly space velocity). Open symbols are end points at same residence time as start of experiment. Conditions: 210 °C; 20 bar; GHSV reduced by increasing flow rate in steps of 25 mL/min from 250 mL/min every 24 h. Data are from Lillebø [34].

An interesting deduction from these data is extrapolation to obtain an estimate for the primary olefin and paraffin termination products in FT-synthesis. The following procedure was adapted: C_3 o/p ratios at 30% conversion were fitted and extrapolated to approach no hydrogen in the feed. The obtained figure was corrected for secondary hydrogenation with time; see trendlines in Figure 3. Finally, minor correction took into account intraparticle diffusion [7]. The final result indicates that ca. 90% of termination is to propene and 10% to propane. Although there are uncertainties involved, it is clear that olefins are dominating termination products in FTS, but that some paraffins most likely also are produced directly. A final comment to Figure 3 concerns the open markers obtained at the end

of each experiment by reverting to the initial GHSV. Lower CO conversion shows deactivation but, simultaneously, the o/p ratio follows the trendline in spite of no further reduction in residence time. A deactivated catalyst evidently suppresses olefin hydrogenation, as discussed in some more detail below.

2.2. Olefin/Paraffin Response to Vapor Pressure of Water

Water is a product of the FT reaction and has significant effect on the amount of produced olefins. Obviously, the vapor pressure of water varies with CO conversion. Additional effects are found when water is part of the feed to the reactor, and one focus of the present study is on the influence of water on FT performance and the olefin to paraffin ratio by adding water during the run. The procedure and effect for the Cα catalyst is shown in Figure 4. The run is divided into five periods A–E:

A. Synthesis gas with flow rate 250 mL/min.
B. Synthesis gas with reduced space velocity to give an initial CO conversion of 45–50% at 30 h time-on-stream (TOS).
C. Keeping the synthesis gas flow-rate from period B and adding water vapor to give 21% water vapor pressure at the reactor inlet.
D. Increasing the water vapor pressure to 35%.
E. Returning to the conditions of period B.

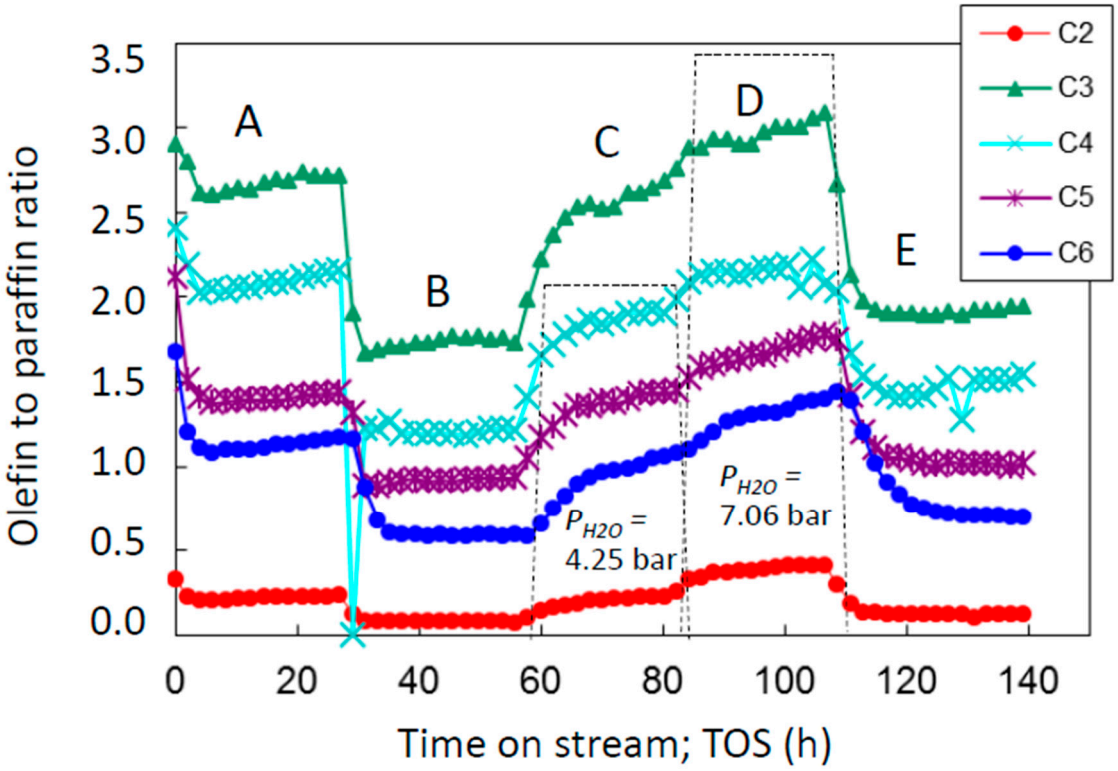

Figure 4. C-C_6 olefin to paraffin ratio for catalyst Cα at varying process conditions. A: Pre-defined space velocity; B: 45–50% conversion; C: added water; D: high water level; E: same GHSV as in period B. Conditions: H_2/CO = 2.1; 210 °C; 20 bar.

This procedure is compatible with previous reports on the effect of water for γ-alumina, silica, titania, and carbon nanofiber, with or without rhenium promoter [11,35,36]. Moreover, the qualitative responses are the same for all these catalysts meaning that the gross effect of changing residence time or water pressure in feed is independent of the catalyst formulation. Plots for CO conversion in the A to E periods for the present catalysts have been published [2,3].

Development in o/p ratio with TOS is rationalized in the following. The initial ratio is dictated by a given space velocity. In this period, as in all subsequent periods, there is a slight increase in relative olefin concentration with time. This trend is ascribed to deactivation, either sintering or oxidation of small crystallites [2]. Sintering is most pronounced in period A, while oxidation takes place mainly in periods C and D when water is added. Several processes occur in parallel during deactivation. Lower conversion due to deactivation in a given test period means less water in the syngas and more hydrogen available for hydrogenation. Still, it is observed that the o/p ratio increases in all periods. Reduced conversion is, however, counteracted by changes in cobalt morphology. First, fewer cobalt sites will become available for hydrogenation. More important is probably that larger and more regular metal crystallites (more ideal stacking, fewer strains and distortions) favor formation of CH_x polymerization monomers at the expense of hydrogen [16]. GHSV is reduced in period B to achieve the targeted 45% CO conversion. Longer residence time for secondary hydrogenation of olefins far outweighs higher conversion and water production, resulting in a distinct drop in o/p. Adding significant amounts of water to the feed in periods C and D enhances CO activation according to the water assisted CO activation mechanism [4], favoring monomer and water coverage on active sites at the expense of hydrogen; thereby depressing olefin hydrogenation. In period E, the syngas flow is returned to period B conditions; the lifted o/p ratio thus confirming that deactivation disfavors olefin hydrogenation.

Plateau data in Figure 4 for each period is plotted as function of chain length in Figure 5. Low o/p for C_2 and the general declining trend with chain length from C_3 are well known, as for instance plotted up to C_{15} for condition similar to period B [17]. It is generally known for hydrogenation of olefins that reactivity increases with chain length. It is striking that all experimental periods follow the same rate of decline in o/p from C_3 to C_6. The implication might be that residence time, water coverage, CO activation, and deactivation, all impact hydrogenation of olefins in a similar way irrespective of chain length. This seems reasonable as it is just a question of availability of adsorption sites, time and hydrogen. Intra-particle diffusion, expected to be most severe for C_6, does not seem to impact the results for the relatively small catalyst particles used.

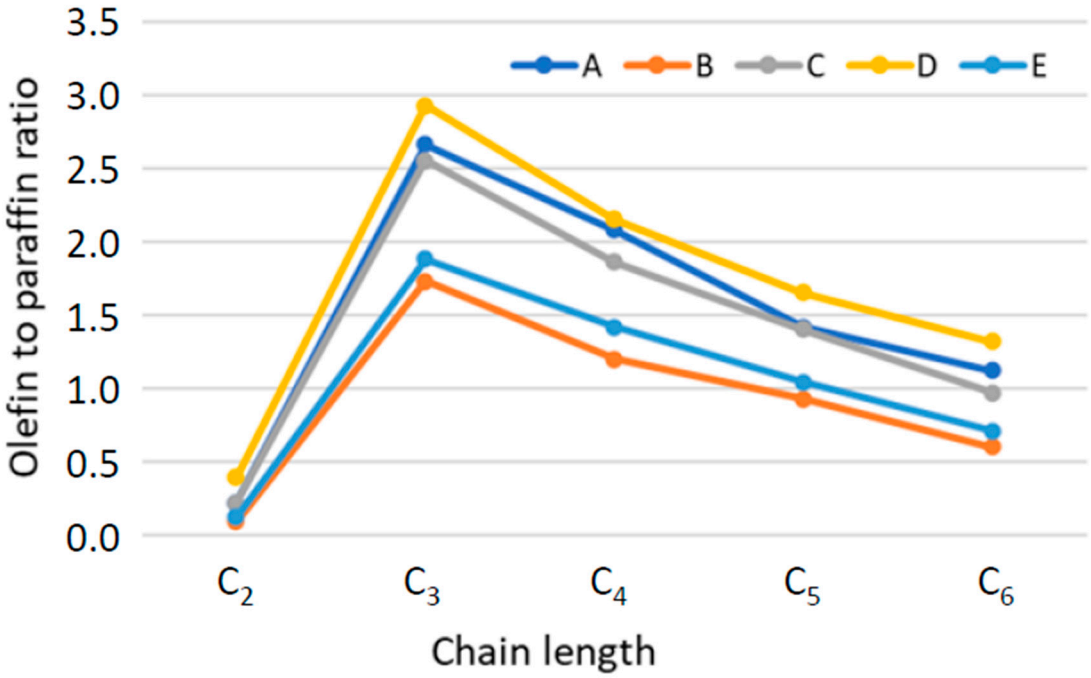

Figure 5. Olefin to paraffin ratio for catalyst Cα at increasing chain lengths. A: Fixed space velocity; B: 45–50% conversion; C: added water; D: high water level; E: same GHSV as in period B.

2.3. Propene/Propane Response to Catalyst Formulation

Comparison of C_3 o/p for three investigated catalysts in all test periods is shown in Figure 6 as function of average partial pressure of water in the fixed-bed reactor. The trends are similar for all catalysts in spite of large variations in pore size and cobalt crystallite size; with one exception. The narrow pore catalyst C3 shows abnormal behavior at high water vapor pressure in period D. Comparably low o/p ratio coincides with lower than expected C_{5+} selectivity [2,37]; ascribed to condensation of water in narrow pores that results in increase in the effective H_2/CO ratio. The effects of partial pressure of water, residence time, and cobalt crystallite size are as discussed above. In addition, there is a residence time effect between the catalysts. This stems from differences in catalyst activity due to higher cobalt dispersion for narrow pores; compensated by GHSV adjustments to achieve 45% CO conversion in period B.

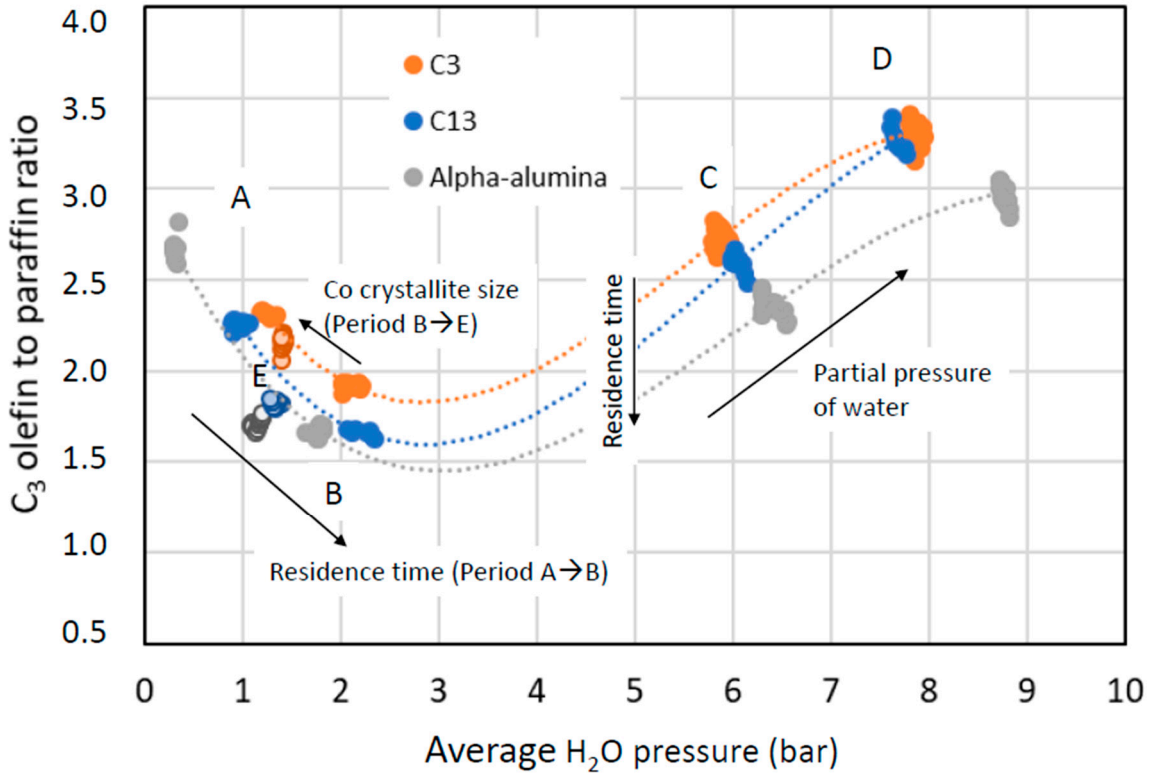

Figure 6. Effect of partial pressure of water on C_3 o/p ratio in the test periods A, B, C, D, and E (open symbols) for cobalt catalysts C_3 and C_{13} on γ-alumina and Cα on α-alumina supports.

It is not trivial to compare and rationalize o/p response between widely different classes of catalysts. Some properties of the present Cα catalyst, and published catalysts with or without Re promoter on γ-alumina, silica, and titania [11], are summarized in Table 1. Pore characteristics of the γ-alumina support are similar to the narrow pore C3 material in Table 2. Some general observations are: Re promoted catalysts always have higher C_{5+} and lower CH_4 selectivities than unpromoted ones; the unpromoted catalysts are less active (GHSV is significantly lower to achieve ±2% units in conversion for test period B).

Table 1. Selectivities and chain propagation probabilities for 12 wt% Co Fischer–Tropsch catalysts at 40–48% CO conversion. Conditions: 210 °C; 20 bar; H_2/CO = 2.1.

Catalyst. Support; Promoter	C_{5+} Selectivity (C%)	CH_4 Selectivity (C%)	Co Size (nm) *	α_1	α_{2+}	C_3 o/p	CO Conv. (%)	GHSV (mL/g_{cat}·h) **	Ref. Exp. Data
γ-Al_2O_3	80.2	9.7	15.2	0.522	0.876	2.3	44.8	2982	Storsæter [11]
γ-$Al2O_3$; 0.5% Re	80.8	8.8	9.4	-	-	2.3	47.6	5960	Storsæter [11]
SiO_2	81.7	9.1	18.1	0.527	0.884	1.1	42.2	3060	Storsæter [11]
SiO_2; 0.5% Re	83.4	8.7	16.4	0.517	0.891	1.4	41.2	4166	Storsæter [11]
TiO_2	82.3	9.8	41.7	0.490	0.893	1.0	39.8	1885	Storsæter [11]
TiO_2; 0.5% Re	84.8	8.9	40.0	-	-	0.8	43.9	3595	Storsæter [11]
α-Al_2O_3; 0.5% Re	84.9	8.6	19.0	0.71	0.906	1.64	43.1	4546	Catalyst Cα

* Based on hydrogen chemisorption. ** Syngas in period B; water comes in addition in periods C and D. – Data not available.

Table 2. Properties of investigated catalysts.

Catalyst Sample	Type of Support	Surface Area (m^2/g)	Pore Diameter (nm)	Pore Volume (cm^3/g)	Pore Size Distribution	Co Size (nm) [a]	GHSV (ml/g·h) @ ca.50% Conv.	Degree of Reduction (%) [b]
C_3	γ-Puralox SCCa 40/195	143	7.1	0.30	Sharp	8.3	9480	56
C_{10}	γ-Puralox SCCa 20/190	149	11.6	0.51	Broad (Low pore size shoulder)	10.2	8947	60
C_{11}	Puralox SCCa 20/190	148	11.6	0.50	Medium broad (Slightly bimodal)	9.5	7536	61
C_{13}	Puralox 190 UHP	92	23.7	0.57	Broad	12.6	7671	71
Cα	α-alumina(84%)	23.5	−150	−0.8	–	19.0	4546	>90

γ: γ-alumina. [a] Based on hydrogen chemisorption. [b] Based on oxygen titration.

The C_3 o/p values for test periods A–D are compared in Figure 7, left. Due to large differences in residence times due to adjustments to achieve similar conversion levels, comparison between the catalysts is not entirely transparent as long residence times favors hydrogenation of olefins. A residence time correction is therefore provided on Figure 7, right; by dividing the o/p ratios with GHSV (L/g_{cat}* h). It is assumed that the hydrogenation rate follows an approximate linear response to GHSV in the observed propene concentration range from 80 to 45%; correct to 98% for a 1st order reaction. Now we are in position to compare catalyst performance under conditions that are close in both water vapor pressure and residence time. The first obvious observation is that all unpromoted catalysts have enhanced corrected o/p ratios compared to their unpromoted counterparts; provisionally meaning that rhenium favors hydrogenation. There is not necessarily a hydrogen spillover effect as Re reduces crystallite size and improves reduction. The resulting higher dispersion favors propene hydrogenation. In fact, direct proportionality was previously found between hydrogen chemisorption and propene chemisorption; with propene occupying four hydrogen sites [38]. We therefore ascribe low o/p ratios for Re promoted catalysts to enhanced number of available sites for hydrogenation. Change in dispersion with Re addition was found for the three supports (Table 1), most distinct for γ-alumina; as also seen for γ-alumina with narrow, medium and wide pore sizes [12]. High C_{5+} selectivity upon Re-promotion and simultaneously reduced corrected o/p ratio are is more challenging to explain. A complicating factor is that C_{5+}-selectivity follows a volcano plot vs. cobalt crystallite size; some details are given in the next section.

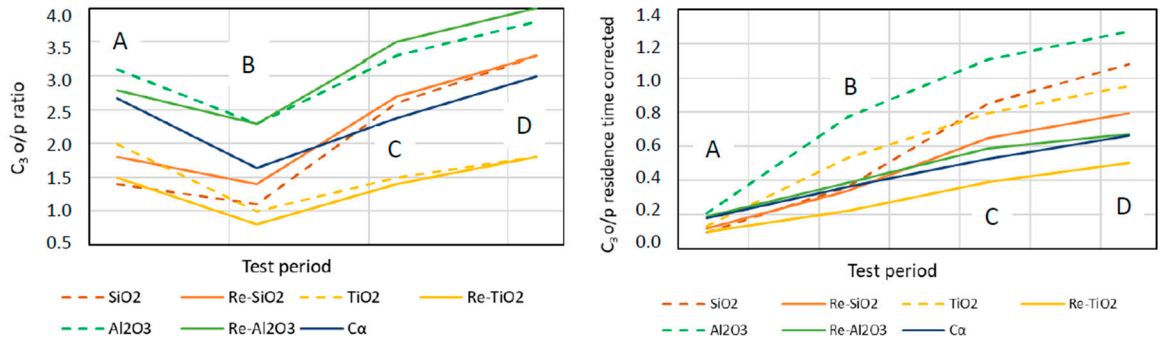

Figure 7. Measured and residence time corrected propene to propane ratio for un-promoted and Re-promoted cobalt catalysts on Al_2O_3, SiO_2, and TiO_2. Periods A, B, C, and D are as in Figure 4. Data are from Storsæter et al. [11].

Another feature of the residence time corrected plot in Figure 7 is that the Re-promoted catalysts have fairly close o/p ratios; with titania favoring some additional hydrogenation. The latter is unexpected due to the very large particle size, in other words, low dispersion, from hydrogen chemisorption. Too low measured hydrogen-based dispersion for cobalt on titania has been described in several reports, and have been attributed to strong-metal-support-interaction (SMSI) with migration of a TiO_x sublayer on cobalt [39,40]. A related complexity in comparing different catalysts is the effect of impurities. In particular alkali and alkaline earth metals impact FT performance, and the inherent concentrations of these elements are known to vary considerably between material classes, producers, and manufacturing methods. In a study of adding Na or Ca to a C11 type catalyst (Co on medium pore γ-alumina; Table 1) up to 1000 ppm, sodium showed increase in C_3 o/p from 2.43 to 2.64 while Ca exhibited a decrease from 2.65 to 2.13 [38]. These trends were in both cases concurrent with variations in C_{5+} selectivity at the same CO conversion, in line with low hydrogenation activities for high o/p ratio and C_{5+} selectivity. In both cases, however, CO reaction rate decreased gradually with impurity concentration. The results were interpreted in terms of an electronic effect as blocking of sites hardly was sufficient to explain the observations.

2.4. Correlations between o/p and C_{5+} Selectivity

There is positive correlation between C_{5+} selectivity and o/p ratio for a given catalyst support at constant CO conversion by varying cobalt crystallite size [18]: see Figure 8. This relationship seems reasonable as both parameters increase when the surface coverage of hydrogen decreases. It follows that, up to a certain threshold, larger cobalt crystallites favor CH_x monomer concentration in expense of hydrogen. However, there are further considerations that need to be addressed. The GHSV is adjusted to ca. 45% conversion to account for variations in cobalt surface area and turn-over-frequency. The available cobalt surface area decreases with crystallite size, while TOF and C_{5+} selectivity are reported to follow volcano type plots with maximum around 8–10 nm [14,41]. No attempt has been made to decouple these effects here. Nevertheless, the two blue markers in the figure are significant. These represent the largest crystallite sizes of 12 and 14 nm, respectively: well past the volcano peak in selectivity [14]. Accordingly, the C_{5+} selectivity is reduced simultaneously as the GHSV is turned down; thus, decreasing o/p. In other words, the o/p vs. C_{5+} relationship is not as trivial as it appears at first sight, and caution should be taken using o/p as a parameter for improving long chain selectivity.

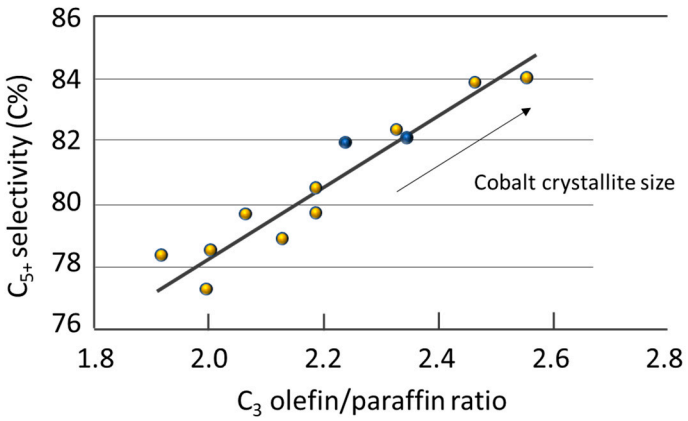

Figure 8. Correlation between C_{5+} selectivity and C_3 o/p ratio at 43–46% CO conversion for catalysts C11′ (C11 version without Re) by varying cobalt crystallite size. Diethylene glycol was added during incipient wetness impregnation. Data are from reference [18]. Blue markers: see text.

The effect of deactivation was mentioned above, and a more detailed analysis of what is happening in period C, when water was first added, is shown in Figure 9. Indeed, o/p and C_{5+} are following each other. It is presumed that small cobalt crystallites oxidize as CO conversion drops with TOS. The remaining larger crystallites are more favorable for suppressing hydrogenation of olefins and producing longer hydrocarbon chains. The observed decline in C_{5+} at the end of period C correlates with the previously found volcano plot as crystallite size increases beyond a certain threshold from the initial value of 8.3 nm; Table 1. The reason for this effect, however, is unexplained; it appears that larger cobalt crystals have more ideal surfaces with less appropriate sites available for activation and polymerization.

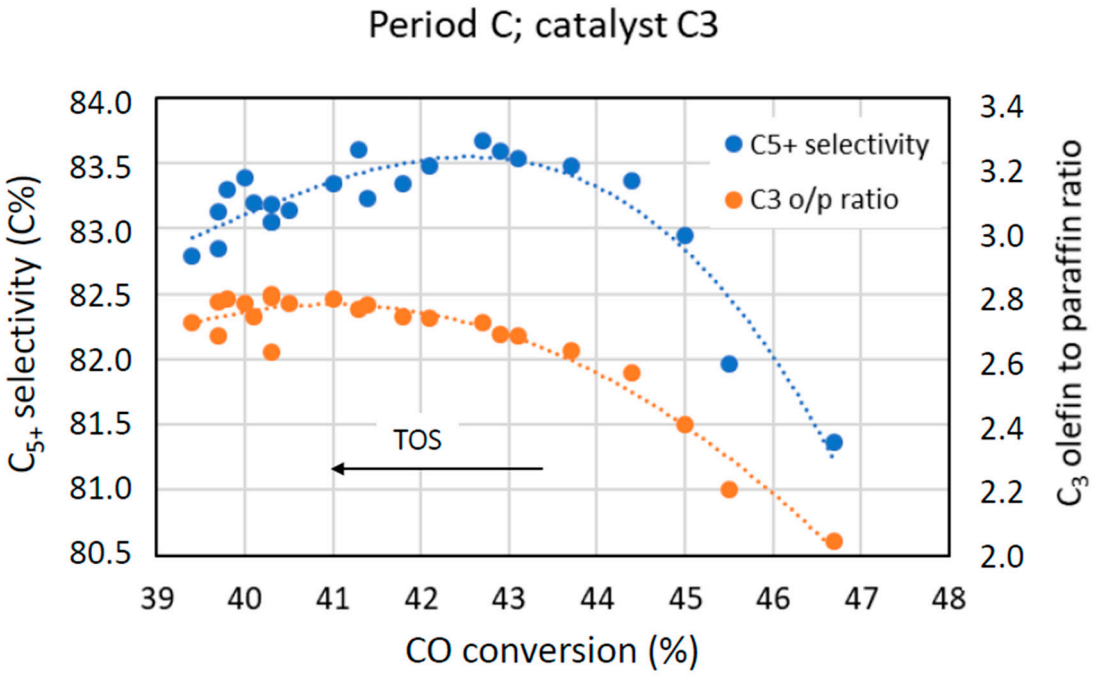

Figure 9. Deactivation behavior in period C for catalyst C3.

Further insight into o/p water responses is gained from transients in periods C, D, and E when water is added or removed; see Figure 10 for a narrow and medium pore size support. From the figure it is obvious that o/p correlates positively with C_{5+} selectivity. Looking at the start of periods C and D, when water is added and gradually penetrates the pores, it appears that water enhances monomer formation and suppresses hydrogenation, as noted above.

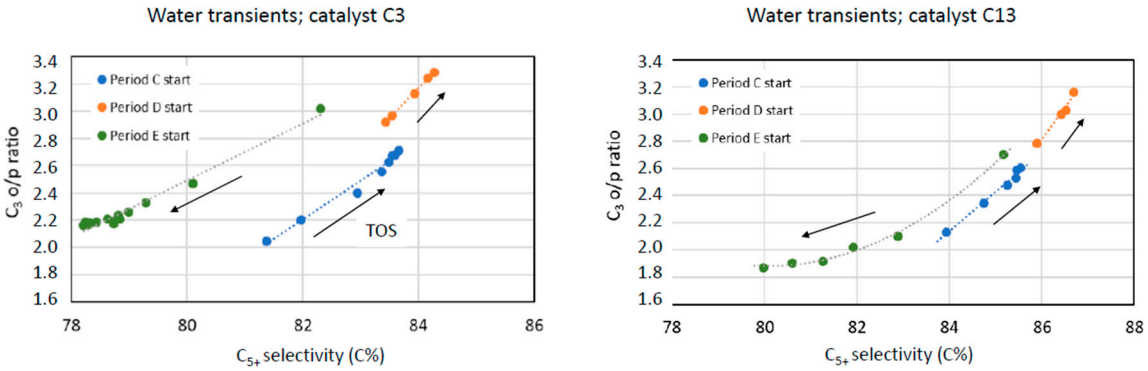

Figure 10. C_3 o/p ratio as a function of C_{5+} selectivity for water transients of catalysts C_3 and C_{13}. Time-on-stream (TOS) directions in periods C, D, and E are indicated.

In terms of ASF α_n-values, higher concentration of long hydrocarbon chains may translate into increase in α_1;

$$\alpha_1 = r_{p1}/(r_{p1} + r_{t1}) \quad (2)$$

where r_{p1} is the rate of the C_1 to C_2 chain initiation reaction and r_{t1} is r_{CH4}; in other words, rate of methane formation. These reactions are proposed to be [4],

$$CH_x^* + (4 - x)\, H^* \rightarrow CH_4 \qquad \text{methanation} \quad (3)$$

$$CH^* + CH_2^* \rightarrow CHCH_2^* \qquad \text{initiation} \quad (4)$$

However, the arguments are valid for other variations involving CH_x* monomers. Indeed, increase of α_1 was found to be the main reason for creation of longer FT hydrocarbon chains in the works of Lögdberg et al. and Todic et al. [6,27,42]. Water presumably displaces hydrogen on the surface, thereby suppressing termination to methane and olefin hydrogenation. Simultaneously, the initiation reaction is favored due to water activating CO. It was found that it is particularly water that contributes to increase in α_1 while pore sizes, in other words, cobalt crystallite size, mainly enhances higher α-values [2,3]. Nevertheless, α-alumina is particularly effective in increasing α_1; see Table 1, but without any extraordinary o/p response; cf. the α_1 values for γ-alumina and α-alumina. This lower than expected o/p ratio for catalysts on α-alumina is probably due to low activity that requires long residence times to achieve the targeted conversion.

Water is removed from the feed in period E, but it takes 10–20 min. until the effect levels out; compare Figures 4 and 10. It is necessary for water to desorb and diffuse from the catalyst pellets. This time span is ca. twice compared to what is needed for saturation when water is added. By comparing dry conditions at the end of the transient period E with start of period C, the o/p ratios appear fairly similar but there is large negative shift in C_{5+} selectivity due to deactivation and consequently lower water partial pressure in period E. In fact, o/p increases from catalyst C13 to C3, as seen more clearly in Figure 6, as a result of lower GHSV. Most distinct is the shift in the position of the E transient toward higher o/p values when water is depleted from the narrow pore C3 catalyst; a result of deactivation and crystallite growth that is more severe for 8.3 nm crystallites compared to 12.6 nm; cf. Table 2.

3. Materials and Methods

3.1. Catalyst Preparation

Laboratory catalysts were prepared as described previously [10–12]. One α-Al_2O_3 support was prepared by calcination of γ-Al_2O_3 (Puralox SCCa 45/190; Sasol GmbH) for 16 h. The catalyst oxide precursor was prepared by one-step incipient wetness co-impregnation with an aqueous solution of cobalt nitrate hexahydrate and perrhenic acid. Before impregnation, the support (53–90 μm) was calcined under air at 500 °C for typically 10 h in a static furnace. The catalysts contain a nominal amount of 20 wt% cobalt and 0.5 wt% Re, as calculated assuming reduced catalyst with complete reduction of cobalt. ICP analysis of calcined samples showed cobalt content in the 16.3–18.9 wt% range and rhenium between 0.36 and 0.42 wt%. The catalyst precursor was dried in a stationary oven at 110–120 °C for 3 h; followed by calcination at 300 °C for 16 h, with a heating rate of 2 °C to the holding temperature. Three catalysts were prepared and numbered as shown in Table 1 and in accordance with previous study [10]. The Cα α-alumina sample corresponds to Cα_1 [3].

3.2. Catalyst Characterization

Key characterization data are found in Table 2. Nitrogen adsorption/desorption isotherms (Micromeritics TriStar 3000, Norcross, GA 30093, USA) were measured after outgassing at 300 °C overnight. The surface area was calculated from the Brunauer–Emmett–Teller (BET) equation, and total pore volume and pore size distribution were found by applying the Barrett–Joyner–Halenda (BJH) method. The nitrogen desorption branch was chosen for pore size analysis. Hydrogen adsorption isotherms were obtained after evacuation 40 °C for 1 h followed by reduction in hydrogen for 6 h at 350 °C. Chemisorbed hydrogen was found from the isotherm recorded in the pressure interval 20 to 510 mmHg and extrapolation to zero pressure. Cobalt crystallite size was calculated by assuming spherical particles and no contribution from the rhenium promoter. Oxygen titration of reduced samples was performed by adding a series of oxygen pulses at 400 °C. Degree of reduction (DOR) was calculated assuming that metallic cobalt oxidized to Co_3O_4. Powder X-ray diffraction patterns (Siemens D5005, 80333 Munich, Germany) and temperature-programmed reduction (TPR) (in house assembled equipment) can be found in previous reports [10–12].

As shown in Table 1, the investigated catalysts span wide ranges of pore diameters, pore size distributions, and cobalt particle sizes; giving very different Fischer–Tropsch performances in terms of activities, selectivities, and water responses. There is positive correlation between cobalt crystallite size and pore size, with slightly enhanced crystallite sizes for supports with very broad pore size distributions [2].

3.3. Fixed-Bed Catalyst Testing

FT reactions were conducted in fixed-bed reactors (stainless steel, 10 mm inner diameter produced in house). Samples were sieved (53–90 μm), and 1–2 g were diluted with inert silicon carbide particles in order to improve temperature distribution. An aluminum jacket was placed outside the reactor to secure isothermal conditions. Catalysts were reduced in situ in hydrogen at ambient pressure while the temperature was increased at 1 °C/min to 350 °C. After 16 h of reduction, the reactor was cooled to 170 °C, pressurized to 20 bar, and synthesis gas of molar ratio $H_2/CO = 2.1$ with 3% N_2 as an internal standard was added. The temperature was then increased slowly to the reaction temperature of 210 °C. Space velocity was adjusted to give carbon monoxide conversion level between 45 and 50 percent after 26 h time-on-stream (TOS). Water was vaporized, heated to reaction temperature and added to the feed at intervals in two concentration levels, 4.25 bar and 7.06 bar; simulating 46 and 64% conversion at the inlet, respectively.

Liquid products were removed in a cold trap, while heavy hydrocarbons were collected in a heated trap. The effluent gaseous product was analyzed for hydrogen, nitrogen, carbon monoxide, carbon dioxide, water, and C_1 to C_9 hydrocarbons, using an HP5890 gas chromatograph equipped with thermal conductivity detector (TCD) and flame ionization detector (FID). C_{5+} selectivity was calculated by subtracting C_1–C_4 hydrocarbons and carbon dioxide from the total mass balance. Activity is reported as the hydrocarbon formation rate ($g_{\text{hydrocarbon}}/(g_{\text{catalyst}}h)$). The precision of the activity is 3% (2σ).

4. Conclusions

The olefin to paraffin ratio is a powerful tool in analyzing selectivity effects in cobalt Fischer–Tropsch synthesis. This ratio responds to process conditions and catalyst formulation and is directly linked to the mechanism of the FT reaction. The o/p ratio is particularly sensitive to flow rate and flow conditions; the latter meaning that the ratio serves as a quality measure for packing of fixed-bed reactors (not shown in the present work).

For a given catalyst, the C_3 olefin to paraffin ratio increases with:

- Reduction in residence time by increasing space velocity; note that this effect is slightly counteracted by simultaneous reduction in CO conversion as well as indigenous production of water.
- Added water to the syngas feed.
- Reduction in H_2/CO ratio.
- Reduction in total pressure or temperature. These effects are moderate (not documented in the present work).

At constant process condition (pressure, temperature, CO conversion, H_2/CO ratio close to consumption ratio), the C_3 olefin to paraffin ratio increases with (for):

- C_{5+} selectivity for the same support by increasing cobalt crystallite size. Details need to be verified around the peak of the volcano plot.
- Reduction in cobalt stacking faults and lattice defects.
- Absence of promoter (Re).
- Deactivation.
- Reduction in catalyst particle (pellet) size.
- Decreasing carbon number until C_3.

The effect of support on o/p is more complex as pore size, type of material, and SMSI play a role. The above effects on the o/p ratio are explained by:

- Olefins as the primary product of cobalt Fischer–Tropsch synthesis.
- Paraffins being mostly produced by secondary hydrogenation of olefins.
- Hydrogen surface coverage being suppressed by water.
- Conditions favoring high formation rate of CH_x monomers suppress hydrogen coverage.
- Transport limitations favor olefin hydrogenation.

Light hydrocarbon olefin to paraffin ratio is a powerful tool for analyzing and understanding low-temperature cobalt Fischer–Tropsch synthesis and the nature of the investigated catalyst. Deeper insight needs further work in both development of mechanism and kinetics as well as surface science. More data for a multitude of catalyst formulations are needed in order for the o/p ratio to be an effective tool in catalyst design.

Author Contributions: Conceptualization: E.R. and A.H.; methodology: E.R.; validation: J.Y.; experimental investigation: Ø.B.; original draft: E.R.; writing—review and editing: J.Y. and A.H. All authors have read and agreed to the published version of the manuscript.

Funding: This research received no external funding.

Conflicts of Interest: The authors declare no conflict of interest.

References

1. Rytter, E.; Holmen, A. Perspectives on the effect of water in cobalt fischer–Tropsch synthesis. *ACS Catal.* **2017**, *7*, 5321–5328. [CrossRef]
2. Rytter, E.; Borg, Ø.; Tsakoumis, N.; Holmen, A. Water as key to activity and selectivity in Co Fischer-Tropsch synthesis: γ-Alumina based structure-performance relationships. *J. Catal.* **2018**, *365*, 334–343. [CrossRef]
3. Rytter, E.; Borg, Ø.; Enger, B.C.; Holmen, A. α-Alumina as catalyst support in Co Fischer-Tropsch synthesis and the effect of added water; encompassing transient effects. *J. Catal.* **2019**, *373*, 13–24. [CrossRef]
4. Rytter, E.; Holmen, A. Consorted vinylene mechanism for cobalt Fischer-Tropsch synthesis encompassing water or hydroxyl assisted CO-activation. *Top. Catal.* **2018**, *61*, 1024–1034. [CrossRef]
5. Oosterbeek, H.; van Bavel, A.P. Effect of CO coverage on the product slate in FTS. In Proceedings of the 11th Natural Gas Conversion Symposium, Tromsø, Norway, 5–9 June 2016. Abstract 992.
6. Lögdberg, S.; Yang, J.; Lualdi, M.; Walmsley, J.C.; Järås, S.; Boutonnet, M.; Blekkan, E.A.; Rytter, E.; Holmen, A. Further insights into methane and higher hydrocarbons formation over cobalt-based catalysts with γ-Al_2O_3, α-Al_2O_3 and TiO_2 as support materials. *J. Catal.* **2017**, *352*, 515–531. [CrossRef]
7. Rytter, E.; Eri, S.; Skagseth, T.H.; Schanke, D.; Bergene, E.; Myrstad, R.; Lindvåg, A. catalyst particle size of cobalt/rhenium on porous alumina and the effect on Fischer−Tropsch catalytic performance. *Ind. Eng. Chem. Res.* **2007**, *46*, 9032–9036. [CrossRef]
8. Shi, B.; Davis, B.H. Fischer–Tropsch synthesis: The paraffin to olefin ratio as a function of carbon number. *Catal. Today* **2005**, *106*, 129–131. [CrossRef]
9. Patzlaff, J.; Liu, Y.; Graffmann, C.; Gaube, J. Interpretation and kinetic modeling of product distributions of cobalt catalyzed Fischer–Tropsch synthesis. *Catal. Today* **2002**, *71*, 381–394. [CrossRef]
10. Borg, Ø.; Eri, S.; Storsæter, S.; Blekkan, E.A.; Wigum, H.; Rytter, E.; Holmen, A. Fischer–Tropsch synthesis over γ-alumina-supported cobalt catalysts: Effect of support variables. *J. Catal.* **2007**, *248*, 89–100. [CrossRef]
11. Storsæter, S.; Borg, Ø.; Blekkan, E.A.; Tøtdal, B.; Holmen, A. Fischer-Tropsch synthesis over re-promoted co supported on Al_2O_3, SiO_2 and TiO_2: Effect of water. *Catal. Today* **2005**, *100*, 343–347. [CrossRef]
12. Borg, Ø.; Hammer, N.; Eri, S.; Lindvåg, O.A.; Myrstad, R.; Blekkan, E.A.; Rønning, M.; Rytter, E.; Holmen, A. Fischer-Tropsch synthesis over un-promoted and re-promoted γ–Al2O3 supported cobalt catalysts with different pore sizes. *Catal. Today* **2009**, *142*, 70–77. [CrossRef]
13. Hilmen, A.-M.; Bergene, E.; Lindvåg, O.A.; Schanke, D.; Eri, S.; Holmen, A. Fischer-Tropsch synthesis using monolithic catalysts. *Stud. Surf. Sci. Catal.* **2000**, *130*, 1163–1168.
14. Rane, S.; Borg, Ø.; Yang, J.; Rytter, E.; Holmen, A. Effect of alumina phases on hydrocarbon selectivity in Fischer-Tropsch synthesis. *Appl. Catal. A Gen.* **2010**, *388*, 160–167. [CrossRef]

15. Rane, S.; Borg, Ø.; Rytter, E.; Holmen, A. Relation between hydrocarbon selectivity and cobalt particle size for alumina supported cobalt Fischer-Tropsch catalysts. *Appl. Catal. A Gen.* **2012**, *437–438*, 10–17. [CrossRef]
16. Tsakoumis, N.E.; Patanou, E.; Lögdberg, S.; Johnsen, R.E.; Myrstad, R.; van Beek, W.; Rytter, E.; Blekkan, E.A. Structure-performance relationships on co-based Fischer-Tropsch synthesis catalysts: The more defect-free, the better. *ACS Catal.* **2019**, *9*, 511–520. [CrossRef]
17. Enger, B.C.; Fossan, Å.-L.; Borg, Ø.; Rytter, E.; Holmen, A. Modified alumina as catalyst support in the Fischer-Tropsch synthesis. *J. Catal.* **2011**, *284*, 9–22. [CrossRef]
18. Borg, Ø.; Dietzel, P.D.C.; Spjelkavik, A.I.; Tveten, E.Z.; Walmsley, J.C.; Eri, S.; Holmen, A.; Rytter, E. Fischer-Tropsch synthesis: Cobalt particle size and support effects on intrinsic activity and product distribution. *J. Catal.* **2008**, *259*, 161–164. [CrossRef]
19. Iglesia, E.; Reyes, S.C.; Madon, R.J.; Soled, S.L. Selectivity control and catalyst design in the Fischer-Tropsch synthesis: Sites, pellets, and reactors. In *Advances in Catalysis*; Eley, H.P.D.D., Paul, B.W., Eds.; Academic Press: San Diego, CA, USA, 1993; Volume 39, pp. 221–301.
20. Komaya, T.; Bell, A.T. Estimates of rate coefficients for elementary processes occurring during Fischer-Tropsch synthesis over $RuTiO_2$. *J. Catal.* **1994**, *146*, 237–248. [CrossRef]
21. Herington, E.F.G. The Fischer-Tropsch synthesis considered as a polymerization reaction. *Chem. Ind.* **1946**, *65*, 346–347.
22. Iglesia, E.; Reyes, S.C.; Madon, R.J. Transport-enhanced α-olefin readsorption pathways in Ru-catalyzed hydrocarbon synthesis. *J. Catal.* **1991**, *129*, 238–256. [CrossRef]
23. Dinse, A.; Aigner, M.; Ulbrich, M.; Johnson, G.R.; Bell, A.T. Effects of Mn promotion on the activity and selectivity of Co/SiO_2 for Fischer-Tropsch synthesis. *J. Catal.* **2012**, *288*, 104–114. [CrossRef]
24. Das, T.K.; Conner, W.; Jacobs, G.; Li, J.; Chaudhari, K.; Davis, B.H. Fischer-Tropsch synthesis: Effect of water on activity and selectivity for a cobalt catalyst. *Stud. Surf. Sci. Catal.* **2004**, *147*, 331–336.
25. Aaserud, C.; Hilmen, A.-M.; Bergene, E.; Eri, S.; Schanke, D.; Holmen, A. Hydrogenation of propene on Cobalt Fischer–Tropsch catalysts. *Catal. Lett.* **2004**, *94*, 171–176. [CrossRef]
26. Schanke, D.; Eri, S.; Rytter, E.; Aaserud, C.; Hilmen, A.-M.; Lindvåg, O.A.; Bergene, E.; Holmen, A. Fischer-Tropsch synthesis on cobalt catalysts supported on different aluminas. *Stud. Surf. Sci. Catal.* **2004**, *147*, 301–306.
27. Todic, B.; Ma, W.; Jacobs, G.; Davis, B.H.; Bukur, D.B. Effect of process conditions on the product distribution of Fischer–Tropsch synthesis over a re-promoted cobalt-alumina catalyst using a stirred tank slurry reactor. *J. Catal.* **2014**, *311*, 325–338. [CrossRef]
28. Yang, J.; Ma, W.; Chen, D.; Holmen, A.; Davis, B.H. Fischer–Tropsch synthesis: A review of the effect of CO conversion on methane selectivity. *Appl. Catal. A Gen.* **2014**, *470*, 250–260. [CrossRef]
29. Zimmerman, W.; Bukur, D.; Ledakowicz, S. Kinetic model of Fischer-Tropsch synthesis selectivity in the slurry phase. *Chem. Eng. Sci.* **1992**, *47*, 2707–2712. [CrossRef]
30. Shi, B.; O'Brien, R.J.; Bao, S.; Davis, B.H. Mechanism of the isomerization of 1-alkene during iron-catalyzed Fischer-Tropsch synthesis. *J. Catal.* **2001**, *199*, 202–208. [CrossRef]
31. Shi, B.; Jacobs, G.; Sparks, D.; Davis, B.H. Fischer-Tropsch synthesis: Accounting for chain length phenomena. *Fuel* **2005**, *84*, 1093–1098. [CrossRef]
32. Krishnamoorthy, S.; Tu, M.; Ojeda, M.P.; Pinna, D.; Iglesia, E. An investigation of the effects of water on rate and selectivity for the Fischer–Tropsch synthesis on cobalt-based catalysts. *J. Catal.* **2002**, *211*, 422–433. [CrossRef]
33. Yang, J.; Shafer, W.D.; Pendyala, V.R.R.; Jacobs, G.; Chen, D.; Holmen, A.; Davis, B.H. Fischer-Tropsch synthesis: Using deuterium as a tool to investigate primary product distribution. *Catal. Lett.* **2014**, *144*, 524–530. [CrossRef]
34. Lillebø, A.H. Conversion of Biomass Derived Synthesis Gas into Liquid Fuels via the Fischer–Tropsch Synthesis Process: Effect of Alkali and Alkaline Earth Metal Impurities and CO Conversion Levels on Cobalt Based Catalysts. Ph.D. Thesis, NTNU, Trondheim, Norway, 2014.
35. Borg, Ø.; Yu, Z.; Chen, D.; Blekkan, E.A.; Rytter, E.; Holmen, A. The effect of water on the activity and selectivity for carbon nanofiber supported cobalt Fischer–Tropsch catalysts. *Top. Catal.* **2014**, *57*, 491–499. [CrossRef]

36. Borg, Ø.; Storsæter, S.; Eri, S.; Wigum, H.; Rytter, E.; Holmen, A. The effect of water on the activity and selectivity for γ-alumina supported cobalt Fischer–Tropsch catalysts with different pore sizes. *Catal. Lett.* **2006**, *107*, 95–102. [CrossRef]
37. Rytter, E.; Holmen, A. On the support in cobalt Fischer-Tropsch synthesis—Emphasis on alumina and aluminates. *Catal. Today* **2016**, *275*, 11–19. [CrossRef]
38. Borg, Ø.; Hammer, N.; Enger, B.C.; Myrstad, R.; Lindvåg, O.A.; Eri, S.; Skagseth, T.H.; Rytter, E. Effect of biomass-derived synthesis gas impurity elements on cobalt Fischer-Tropsch catalyst performance including in situ sulfur and nitrogen addition. *J. Catal.* **2011**, *279*, 163–173. [CrossRef]
39. Li, Y.; Fan, Y.; Yang, H.; Xu, B.; Feng, L.; Yang, M.; Chen, Y. Strong metal-support interaction and catalytic properties of anatase and rutile supported palladium catalyst Pd/TiO_2. *Chem. Phys. Lett.* **2003**, *372*, 160–165. [CrossRef]
40. Haller, G.L.; Resasco, D.E. Metal-support interaction: Group VIII metals and reducible oxides. *Adv. Catal.* **1989**, *36*, 173–235.
41. Bezemer, G.L.; Bitter, J.H.; Kuipers, H.P.C.E.; Oosterbeek, H.; Holewijn, J.E.; Xu, X.; Kapteijn, F.; van Dillen, A.J.; de Jong, K.P. Cobalt particle size effects in the Fischer-Tropsch reaction studied with carbon nanofiber supported catalysts. *J. Am. Chem. Soc.* **2006**, *128*, 3956–3964. [CrossRef]
42. Lögdberg, S.; Lualdi, M.; Järås, S.; Walmsley, J.C.; Blekkan, E.A.; Rytter, E.; Holmen, A. On the selectivity of cobalt-based Fischer-Tropsch catalysts: Evidence for a common precursor for methane and long chain hydrocarbons. *J. Catal.* **2010**, *274*, 84–98. [CrossRef]